Synthesis, thermal, dielectric and electro-optic properties of new series of fluorinated hydrogen-bonded liquid crystals

Mouna Derbali, Taoufik Soltani, Ahlem Guesmi, Naoufel Ben Hamadi, Erwann Jeanneau, Yves Chevalier

Synthesis, thermal, dielectric and electro-optic properties of new series of fluorinated hydrogen-bonded liquid crystals

Mouna Derbali[a], Taoufik Soltani[a*], Ahlem Guesmi[b], Naoufel Ben Hamadi[b], Erwann Jeanneau[c], Yves Chevalier[d*]

[a] Université de Tunis El Manar, Faculté des Sciences de Tunis, LR99ES16 Laboratoire Physique de la Matière Molle et de la Modélisation Électromagnétique, 2092 Tunis, Tunisia.
[b] Chemistry Department, College of Science, IMSIU (Imam Mohammad Ibn Saud Islamic University), Riyadh, Kingdom of Saudi Arabia.
[c] Université Claude Bernard Lyon 1, Centre de Diffractométrie Henri Longchambon, 69622 Villeurbanne, France.
[d] Université Claude Bernard Lyon 1, Laboratoire d'Automatique, de Génie des Procédés et de Génie Pharmaceutique, LAGEPP, CNRS UMR 5007, 43 bd 11 Novembre, 69622 Villeurbanne Cedex, France.

Corresponding authors: Yves Chevalier yves.chevalier@univ-lyon1.fr
Taoufik Soltani tawfik_sol@yahoo.fr

Abstract

Two series of hydrogen-bonded liquid crystals (HBLC) were investigated: 4-alkoxy-2,3-difluorobenzoic acids (nOBAFF) with alkoxy chain lengths of n = 7–12 carbon atoms and mixtures of nOBAFF and 4-octyloxybenzoic acid (8OBA). Their phase behavior has been established using differential scanning calorimetry, polarized optical microscopy and X-ray diffraction. At variance with non-fluorinated and monofluorinated homologues, the difluorinated nOBAFF compounds only form SmA and SmC liquid crystalline phases. An additional nematic phase is obtained upon mixing nOBAFF and 8OBA, showing the sequence: Isotropic liquid–Nematic–SmA–SmC–crystalline solid upon cooling from the isotropic phase. All the transition temperatures decrease with increasing alkoxy chain length of nOBAFF, which reveals a decrease of order parameter for longer chains. The dielectric and electro-optic behaviors of the nematic phase of nOBAFF/8OBA mixtures reveal a decrease of the threshold voltage and response time upon increasing the alkyl chain length of nOBAFF.

Keywords: Hydrogen-bonded liquid crystal, Nematic phase, Smectic phases, Dielectric spectroscopy.

Highlights:

- 4-Alkyloxy-2,3-difluorobenzoic acids self-associate as SmA and SmC hydrogen-bonded liquid crystals

- Mixtures of 4-alkoxy-2,3-difluorobenzoic acids and 4-octylloxybenzoic acid display nematic, SmA and SmC phases
- Order parameter, transition temperatures, threshold voltage and response time decrease with increasing alkoxy chain length

1. Introduction

Thermotropic liquid crystals (LCs) have received special attention because of their interesting anisotropic optical and electrical properties. Hydrogen-bonded liquid crystals (HBLCs) are known for their high thermal stability and rich polymorphism [1–4]. Since the first report of the phase behavior of the *n*-alkoxy benzoic acids LCs formed via hydrogen bonding [5], much research work has been made in the synthesis, phase behavior and properties of this class of LCs. Most of these materials, which are divided into symmetric and non-symmetric dimers, exhibit nematic and smectic phases [6–13]. In 1980, the complexes formed via hydrogen bonding between mesogenic benzoic acids and pyridyl-based fragments have been described by Kato and Fréchet [14]. Using this approach, several complex LCs materials including nematic, SmC, and twist bend phases have been reported [15–18].

The impact of the fluorination of the phenyl ring on the mesomorphic behavior and LCs properties has been investigated by several groups [19–22]. It has been found that the properties of hydrogen-bonded materials such as melting point, mesophase morphology, transition temperatures and dielectric properties as well as optical anisotropy are significantly influenced by fluorination. Fluorination of the core unit decreases the transition temperature and mesomorphic stability, which effect are attributed to repulsive interactions between the fluoro substituent and the electronic environment of the diazo bond [23]. Conversely, fluorination of the alkyl chain increases the melting point and mesophase range compared to the non-fluorinated compounds [24]. We have recently reported the interesting electric and electro-optic properties of monofluorinated benzoic acids (nOBAF; *n* is the carbon number) [19,21]. Fluorination improved the properties of these LCs such as widening of the temperature range of the polar nematic phase and enhancement of the dielectric and electro-optic properties compared to the non-fluorinated homologues (nOBA). As an example, 8OBA forms several LC phases at temperatures between the solid crystalline (Cr) and isotropic liquid (I) phases following the sequence Cr–(73.3 °C)–SmC–(98.2 °C)–N–(138.4 °C)–I, whereas the sequence for 8OBAF is Cr–(56.0 °C)–SmF–(75.2 °C)–SmC–(96.6 °C)–N–(116.2 °C)–I [8]. These results motivated the investigation of new difluorinated benzoic acids (nOBAFF) and their mixtures with 8OBA. We herein report the synthesis and phase behavior of a series of nOBAFF (n = 7–12) compounds. Next, mixing nOBAFF and 8OBA allows modifying the phase behavior because intermolecular H-bonding interactions between them yield non-symmetric dimers with high polarity. We investigated the formation of the hydrogen-bonded complexes by IR spectroscopy, and the phase behavior using differential scanning calorimetry (DSC) and

polarized optical microscopy (POM). Finally, electro-optic and dielectric behaviors were studied. The effects of the chain length (*n*) of nOBAFF was discussed.

2. Experimental

2.1. Synthesis

4-Octyloxybenzoic acid (8OBA) was purchased from Sigma-Aldrich. 4-*n*-Alkoxy-2,3-difluorobenzoic acids (nOBAFF) with chain lengths in the range n = 7–12 were synthesized and characterized by NMR spectroscopy. The following example for n = 10 is typical of the synthetic methods used to obtain 2,3-difluoro-4-alkoxybenzoic acid (nOBAFF) compounds. 1-Bromodecane (17 g, 0.077 mol) was added dropwise to a stirred solution of potassium hydroxide (5.8 g, 0.1 mol), water (10 mL), ethanol (100 mL) and 2,3-difluoro-4-hydroxybenzoic acid (10 g, 0.058 mol). The solution was heated under reflux for 3 h. After cooling to room temperature, KOH (4 g, 0.07 mol) in 10 mL of water was added and the mixture was again stirred under reflux for 2 h. Then, KOH (5 g) in 5 mL of water was added to the cold solution and the mixture was heated under reflux for a further 2 h. The solvent was evaporated and the mixture was poured onto crushed ice and HCl (35 %). The solid product was filtered off and recrystallized from absolute ethanol.

2.2. NMR analyses

7OBAFF:

^{1}H NMR (300 MHz, $CDCl_3$), δ (ppm from TMS): 0.816 (t, 3H, $^{3}J_{H–H}$ = 6.7 Hz), 1.212 (8H), 1.784 (quint, 2H, $^{3}J_{H–H}$ = 7.4 Hz), 4.045 (t, 2H, $^{3}J_{H–H}$ = 6.6 Hz), 6.716 (m, 1H, $^{3}J_{H–H}$ = 9.1 Hz, $^{4}J_{H–F}$ = 7.1 Hz, $^{5}J_{H–F}$ = 1.8 Hz), 7.699 (m, 1H, $^{3}J_{H–H}$ = 9.1 Hz, $^{4}J_{H–F}$ = 7.6 Hz, $^{5}J_{H–F}$ = 2.3 Hz)

^{13}C NMR (101 MHz, $CDCl_3$), δ (ppm from TMS): 14.05, 22.57, 25.75, 28.92, 28.94, 31.70, 69.95, 108.34 (d, $^{3}J_{C–F}$ = 3.83 Hz), 110.77 (d, $^{2}J_{C–F}$ = 7.39 Hz), 127.22 (d, $^{3}J_{C–F}$ = 3.37 Hz), 142.03 (dd, $^{1}J_{C–F}$ = 248 Hz, $^{2}J_{C–F}$ = 13.2 Hz), 151.96 (dd, $^{1}J_{C–F}$ = 228 Hz, $^{2}J_{C–F}$ = 11.1 Hz), 153.42 (dd, $^{2}J_{C–F}$ = 8.2 Hz, $^{3}J_{C–F}$ = 3.75 Hz), 168.65 (t, $^{3}J_{C–F}$ = 3.08 Hz, $^{4}J_{C–F}$ = 3.08 Hz).

^{19}F NMR (282 MHz, $CDCl_3$), δ (ppm from $CFCl_3$): −132.47 (d, 1F), −158.17 (d, 1F, $^{3}J_{F–F}$ = 28.2 Hz).

9OBAFF:

^{1}H NMR (300 MHz, $CDCl_3$), δ (ppm from TMS): 0.816 (t, 3H, $^{3}J_{H–H}$ = 6.7 Hz), 1.211 (12H), 1.784 (quint, 2H, $^{3}J_{H–H}$ = 7.4 Hz), 4.045 (t, 2H, $^{3}J_{H–H}$ = 6.6 Hz), 6.716 (m, 1H, $^{3}J_{H–H}$ = 9.1 Hz, $^{4}J_{H–F}$ = 7.1 Hz, $^{5}J_{H–F}$ = 1.8 Hz), 7.699 (m, 1H, $^{3}J_{H–H}$ = 9.1 Hz, $^{4}J_{H–F}$ = 7.6 Hz, $^{5}J_{H–F}$ = 2.3 Hz).

^{13}C NMR (101 MHz, $CDCl_3$), δ (ppm from TMS): 13.92, 22.56, 25.74, 28.94, 29.12, 29.20, 29.38, 31.78, 70.10, 108.62 (d, $^3J_{C–F}$ = 2.83 Hz), 110.96 (d, $^2J_{C–F}$ = 7.06 Hz), 127.10 (d, $^3J_{C–F}$ = 3.98 Hz), 141.61 (dd, $^1J_{C–F}$ = 248 Hz, $^2J_{C–F}$ = 14.1 Hz), 152.15 (dd, $^1J_{C–F}$ = 262 Hz, $^2J_{C–F}$ = 11.5 Hz), 153.38 (dd, $^2J_{C–F}$ = 7.85 Hz, $^3J_{C–F}$ = 3.66 Hz), 168.04 (t, $^3J_{C–F}$ = 3.04 Hz, $^4J_{C–F}$ = 3.04 Hz).
^{19}F NMR (282 MHz, $CDCl_3$), δ (ppm from $CFCl_3$): −132.47 (d, 1F), −158.17 (d, 1F, $^3J_{F–F}$ = 28.2 Hz).

10OBAFF:
^{1}H NMR (300 MHz, $CDCl_3$), δ (ppm from TMS): 0.814 (t, 3H, $^3J_{H–H}$ = 6.7 Hz), 1.206 (14H), 1.784 (quint, 2H, $^3J_{H–H}$ = 7.4 Hz), 4.044 (t, 2H, $^3J_{H–H}$ = 6.6 Hz), 6.716 (m, 1H, $^3J_{H–H}$ = 9.1 Hz, $^4J_{H–F}$ = 7.1 Hz, $^5J_{H–F}$ = 1.8 Hz), 7.699 (m, 1H, $^3J_{H–H}$ = 9.1 Hz, $^4J_{H–F}$ = 7.6 Hz, $^5J_{H–F}$ = 2.3 Hz).
^{13}C NMR (101 MHz, $CDCl_3$), δ (ppm from TMS): 13.93, 22.56, 25.75, 28.94, 29.20, 29.20, 29.43, 29.44, 31.82, 70.10, 108.59 (d, $^3J_{C–F}$ = 2.76 Hz), 110.99 (d, $^2J_{C–F}$ = 7.03 Hz), 127.11 (d, $^3J_{C–F}$ = 4.08 Hz), 141.59 (dd, $^1J_{C–F}$ = 247 Hz, $^2J_{C–F}$ = 14.1 Hz), 152.17 (dd, $^1J_{C–F}$ = 262 Hz, $^2J_{C–F}$ = 11.5 Hz), 153.40 (dd, $^2J_{C–F}$ = 7.35 Hz, $^3J_{C–F}$ = 3.65 Hz), 168.62 (t, $^3J_{C–F}$ = 3.04 Hz, $^4J_{C–F}$ = 3.04 Hz).
^{19}F NMR (282 MHz, $CDCl_3$), δ (ppm from $CFCl_3$): −132.50 (d, 1F), −158.18 (d, 1F, $^3J_{F–F}$ = 28.2 Hz).

11OBAFF:
^{1}H NMR (300 MHz, $CDCl_3$), δ (ppm from TMS): 0.813 (t, 3H, $^3J_{H–H}$ = 6.7 Hz), 1.201 (16H), 1.784 (quint, 2H, $^3J_{H–H}$ = 7.4 Hz), 4.044 (t, 2H, $^3J_{H–H}$ = 6.6 Hz), 6.716 (m, 1H, $^3J_{H–H}$ = 9.1 Hz, $^4J_{H–F}$ = 7.1 Hz, $^5J_{H–F}$ = 1.8 Hz), 7.696 (m, 1H, $^3J_{H–H}$ = 9.1 Hz, $^4J_{H–F}$ = 7.6 Hz, $^5J_{H–F}$ = 2.3 Hz).
^{13}C NMR (101 MHz, $CDCl_3$), δ (ppm from TMS): 13.94, 22.56, 25.75, 28.94, 29.20, 29.24, 29.43, 29.49, 29.52, 31.84, 70.10, 108.60 (d, $^3J_{C–F}$ = 2.71 Hz), 110.98 (d, $^2J_{C–F}$ = 7.06 Hz), 127.10 (d, $^3J_{C–F}$ = 3.85 Hz), 141.60 (dd, $^1J_{C–F}$ = 247 Hz, $^2J_{C–F}$ = 14.0 Hz), 152.16 (dd, $^1J_{C–F}$ = 262 Hz, $^2J_{C–F}$ = 11.5 Hz), 153.39 (dd, $^2J_{C–F}$ = 7.84 Hz, $^3J_{C–F}$ = 3.64 Hz), 168.37 (t, $^3J_{C–F}$ = 3.04 Hz, $^4J_{C–F}$ = 3.04 Hz).
^{19}F NMR (282 MHz, $CDCl_3$), δ (ppm from $CFCl_3$): −132.50 (d, 1F), −158.17 (d, 1F, $^3J_{F–F}$ = 28.2 Hz).

12OBAFF:

^{1}H NMR (300 MHz, $CDCl_3$), δ (ppm from TMS): 0.811 (t, 3H, $^{3}J_{H–H}$ = 6.7 Hz), 1.184 (18H), 1.783 (quint, 2H, $^{3}J_{H–H}$ = 7.4 Hz), 4.044 (t, 2H, $^{3}J_{H–H}$ = 6.6 Hz), 6.721 (m, 1H, $^{3}J_{H–H}$ = 9.0 Hz, $^{4}J_{H–F}$ = 7.0 Hz, $^{5}J_{H–F}$ = 1.7 Hz), 7.697 (m, 1H, $^{3}J_{H–H}$ = 9.0 Hz, $^{4}J_{H–F}$ = 7.6 Hz, $^{5}J_{H–F}$ = 2.3 Hz).

^{13}C NMR (101 MHz, $CDCl_3$), δ (ppm from TMS): 13.94, 22.60, 25.75, 28.95, 29.21, 29.26, 29.44, 29.49, 29.56, 29.57, 31.86, 70.07, 108.57 (d, $^{3}J_{C–F}$ = 2.71 Hz), 111.10 (d, $^{2}J_{C–F}$ = 7.06 Hz), 127.10 (d, $^{3}J_{C–F}$ = 3.85 Hz), 141.59 (dd, $^{1}J_{C–F}$ = 248 Hz, $^{2}J_{C–F}$ = 15.4 Hz), 152.16 (dd, $^{1}J_{C–F}$ = 265 Hz, $^{2}J_{C–F}$ = 12.4 Hz), 153.35 (dd, $^{2}J_{C–F}$ = 7.84 Hz, $^{3}J_{C–F}$ = 3.64 Hz), 168.57 (t, $^{3}J_{C–F}$ = 3.04 Hz, $^{4}J_{C–F}$ = 3.04 Hz).

^{19}F NMR (282 MHz, $CDCl_3$), δ (ppm from $CFCl_3$): −132.50 (1F, d), −158.18 (d, 1F, $^{3}J_{F–F}$ = 28.2 Hz).

The complexes nOBAFF/8OBA were obtained by mixing nOBAFF and 8OBA at 1:1 molar ratio according to the process described in [6]. 8OBA and nOBAFF were firstly dissolved in DMF and both solutions were gathered so as to obtain a mixed solution with 1:1 molar ratio of nOBAFF and 8OBA, part of the DMF was removed under reduced pressure, a white crystalline complex (nOBAFF/OBA) separated and was washed with ethanol. The structures of the studied compounds are shown in Figure 1.

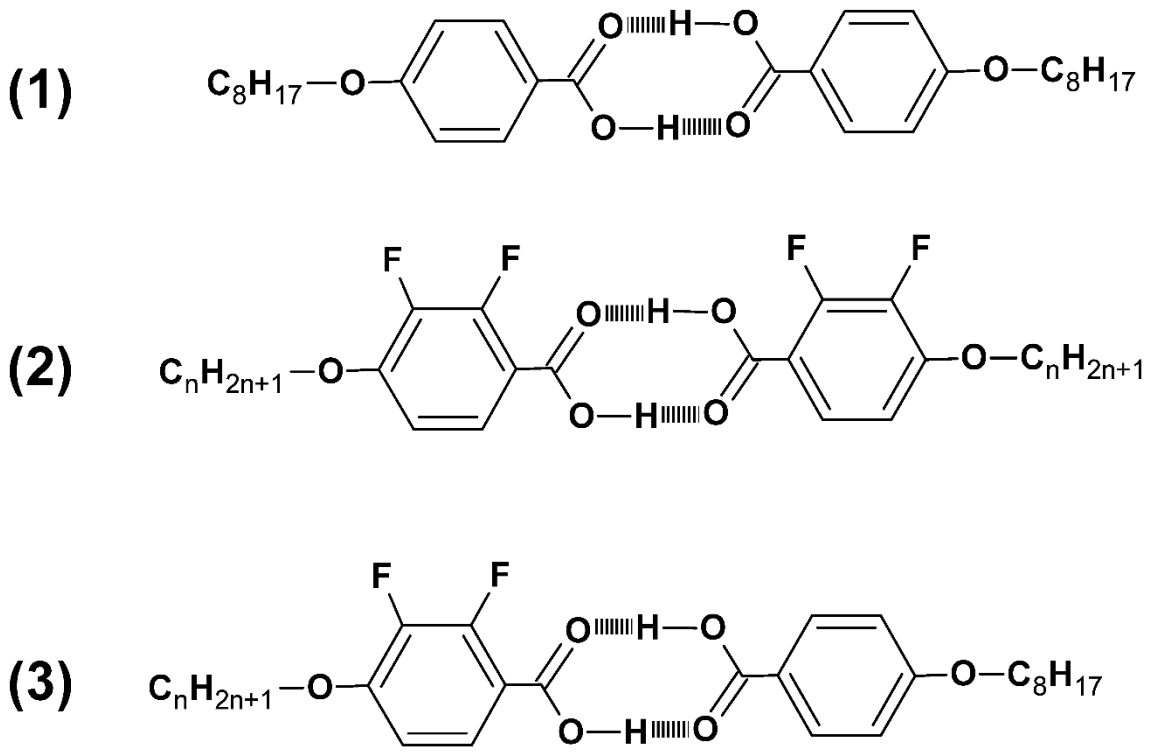

Figure 1. Chemical structure of 8OBA (1), nOBAFF (2) and mixed nOBAFF/8OBA (3); *n* = 7–12.

2.3. Measurement set-up and instruments

The thermal behavior of both series nOBAFF and nOBAFF/8OBA was determined by DSC using a Perkin-Elmer DSC7 operating at heating and cooling rates of 1 °C·min^{-1}. The LC phases were identified by POM using an Olympus BX51 microscope equipped with a Sony digital CCD camera.

Infrared spectra were recorded on dry powders in Attenuated Total Reflectance mode (FTIR-ATR) using a Nicolet™ iS50 FT-IR spectrometer. Spectra were recorded over the wave number range 400–4000 cm^{-1} at a resolution of 4 cm^{-1} and using 32 scans for collecting each spectrum.

X-ray diffraction (XRD) studies were performed at the Centre de Diffraction Henri Longchambon of the Université of Lyon 1 (http://cdalpha.univ-lyon1.fr/) using an Oxford Gemini A Ultra diffractometer with graphite-monochromatized Mo Kα radiation at λ = 0.71073 Å. It was equipped with a Gemini CCD detector. Data reduction was done using the Crysalis Pro software. Glass capillaries of 0.2 mm diameter filled with the samples were heated with a nitrogen gas flow using a Cryostream 700 Plus cooling stage (Oxford Cryosystems) for the collection of scattering patterns at several regulated temperatures. As an important feature of this temperature control setup, the sample is heated in the capillary at the location where the X-ray beam illuminates the sample while the remainder of the sample is kept at lower temperature above and below the region of interest.

In order to investigate dielectric, electro-optical and viscoelastic properties, commercial planar alignment cells (EHC from Japan) were filled with the studied compounds in the isotropic phase by capillary suction. The cells thickness was fixed by 8 µm Mylar wedges and the active area was 0.25 cm^2. The cell was slowly cooled from the isotropic phase into the nematic phase. The temperature was controlled within ± 0.1 °C·min^{-1}.

The dielectric parameters were measured using the impedance/gain phase analyzer (Solartron SI 1260) coupled to 1296 dielectric interface in the frequency range 1–2 MHz. The perpendicular permittivity ($\varepsilon_\perp$) was measured under an applied AC voltage of 0.5 V.

Electro-optical measurements were performed using a polarizing microscope Microscope Eclipse LV100N Nikon, a high-power amplifier and a function generator (Agilent 33220A) that can provides DC electric voltage or a sinusoidal signal with variable amplitude. An electric voltage was applied to the cell connected in series to an external electric resistance of 1 kΩ in order to measure the threshold voltage of the Fréedericksz transition (V_{th}). The response time (τ) is defined as the time required for flipping the molecules from their initial planar orientation to the parallel of the applied electric field when an electric voltage applied to a planar cell is higher than V_{th}. τ was obtained using the square wave drive frequency f = 1 Hz and the amplitude

10 V. A polychromatic light beam of average wavelength 648 nm was chosen as the input signal and the output signal was detected by a photodetector (DET36A Si Biased Detector) connected to a digital storage oscilloscope (Agilent Technologies DSO5052A).

3. Results and discussion

3.1. Phase behavior of nOBAFF

The thermal behavior has been studied by DSC, POM and X-ray diffraction for the whole series of nOBAFF (*n* = 7–12). The behaviors of the members of the series 10OBAFF, 11OBAFF and 12OBAFF have already been studied by Hamdi [25]. It was found that they exhibit SmC, SmF and SmE, respectively. Such dramatic changes of the type of smectic phases upon increasing the chain length by only one carbon atom look rather surprising. The present work extends the series with 7OBAFF and 9OBAFF, allowing a more detailed discussion of the effect of the alkoxy chain length. In the present study, we synthesized nOBAFF (*n* = 7–12) and their phase sequences were obtained using DSC and POM measurements upon heating up to the isotropic phase and cooling down to 20 °C. Figure 2 shows the DSC thermograms of 11OBAFF upon subsequent heating and cooling cycles. LC phases were obtained upon cooling from the isotropic phase. Each compound exhibited SmA and SmC LC phases upon cooling. Two crystalline (Cr_1 and Cr_2) phases were observed both along the heating and cooling cycles. The phase transition temperatures on cooling are shifted with respect to those on heating as it is often the case because nucleation of a new phase on cooling is a slow process. A very slow cooling rate (1°C·min^{-1}) in the DSC experiments revealed the SmA-SmC and Cr_1-Cr_2 transitions, which were not detected at the 5°C·min^{-1} cooling rate of the DSC experiments in [23]. This difference can be explained by the small enthalpy of these transitions. The detection of all transitions require slow cooling and heating processes. The temperature of formation of the crystalline Cr_1 from the LC phases was variable from one experiment to another. The POM experiments allow a much slower cooling rate and equilibration isotherms, so that the transition temperatures are better taken from the POM observations at the active area of the cells. Focal conic texture for SmA and a broken fan-shape texture for SmC phases were observed (Figure 3). In addition, the second order transition SmA-SmC upon heating cycle was detected only by the POM observation. Table 1 and Figure 4 summarize the thermal behavior of nOBAFF. The DSC thermograms of all studied compounds are given in Figure S1 of the SI file.

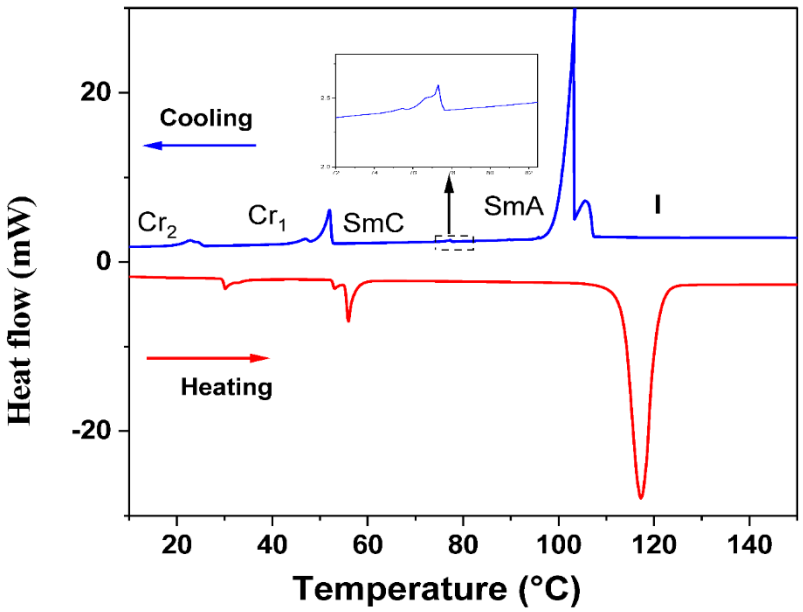

Figure 2. The second heating-cooling DSC trace of 11OBAFF upon heating and cooling.

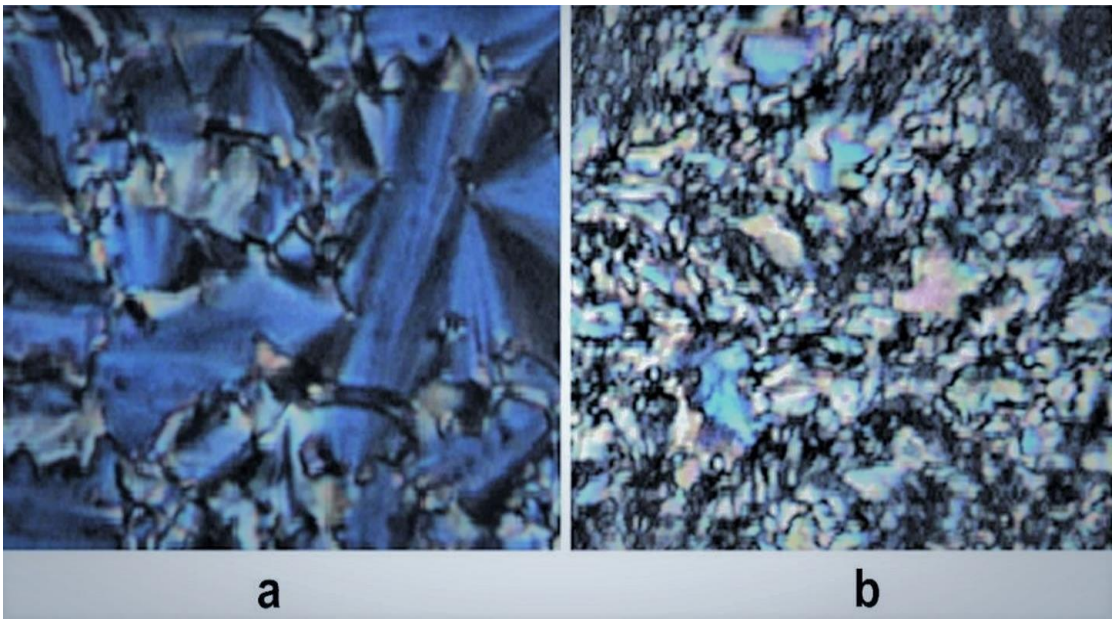

Figure 3. Textures observed by POM on cooling from the isotropic phase; (a) SmA and (b) SmC phases for 10OBAFF.

The X-ray diffraction patterns were measured at different temperatures upon heating up to the isotropic phase and thereafter cooling down to 20 °C. The sole crystalline phase was observed either upon heating till the isotropic phase was reached; and cooling from the isotropic phase directly gave back the crystalline phase. This looks being in contradiction with other experimental results from DSC and POM. This discrepancy is only apparent. Indeed, in the

Cryostream 700 Plus cooling stage, the samples were only locally heated inside the glass capillary (sample holder) in the working area where the X-ray beam illuminated the sample. There was still the crystalline phase remaining in the coldest parts of the capillary. Upon cooling the working area, the crystalline phase could then grow from the crystals present above and below the working area. Growth of the crystalline phase did not require prior nucleation. The combined experiments by DSC, POM and X-ray diffraction strongly suggest that both the crystalline phase Cr_1 and the LC phases can form upon cooling the isotropic phase. The crystalline phase is the thermodynamically stable phase (below the melting temperature measured upon heating) and the LC phases are metastable. This is called monotropic behavior. LC phases are observed upon cooling because their formation from the isotropic phase is faster than that of Cr_1. The confinement in a narrow space between the plates in POM experiments may stabilize the LC phases for long times.

The chain length dependence of thermal stability is depicted in Figure 4. All transition temperatures decrease with respect to *n*. The width of the temperature range of the SmA phase is not affected by *n*. The Cr–SmC transition shows an odd-even effect of the alkoxy chain as it has already been observed in several instances since its early disclosure in 1927 [26,27], both concerning transition temperatures and LC materials properties [28,29].

Table 1. Transition temperatures of nOBAFF observed by POM observations upon cooling and heating.

Substances	Transition temperatures (°C)
7OBAFF	Cooling (°C): Cr_2–(61.8)–Cr_1–(94.1)–SmC–(98.7)–SmA–(111.7)–I Heating (°C): Cr_2–(56.2)–Cr_1–(65)–SmC–(85.8)–SmA–(113.5)–I
9OBAFF	Cooling (°C): Cr_2–(35.1)–Cr_1–(54.8)–SmC–(86.7)–SmA–(108)–I Heating (°C): Cr_2–(24.5)–Cr_1–(44.8)–SmC–(56.1)–SmA–(116.4)–I
10OBAFF	Cooling (°C): Cr_2–(22.7)–Cr_1–(33.7)–SmC–(78.3)–SmA–(110.3)–I Heating (°C): Cr_2–(23.8)–Cr_1–(50.7)–SmC–(80.5)–SmA–(109.8)–I
11OBAFF	Cooling (°C): Cr_2–(22.6)–Cr_1–(52.3)–SmC–(76.8)–SmA–(103.2)–I Heating (°C): Cr_2–(30.0)–Cr_1–(55.8)–SmC–(88.2)–SmA–(117.4)–I
12OBAFF	Cooling (°C): Cr_2–(19.8)–Cr_1–(34.6)–SmC–(80.7)–SmA–(99.1)–I Heating (°C): Cr_2–(26.0)–Cr_1–(50.3)–SmC–(62.8)–SmA–(111.1)–I

It is important to remind that the series of monofluorinated and non-fluorinated homologues display a nematic phase [21,30,31], whereas the difluorinated compounds do not. This is the reason why we believe that the intermolecular interactions between H and F atoms are the predominant driving force in the preferred formation of SmA and SmC phases instead of the nematic phase. So, the appearance of the smectic phases without the nematic phase in this case can be attributed to intermolecular H- - -F hydrogen bonds.

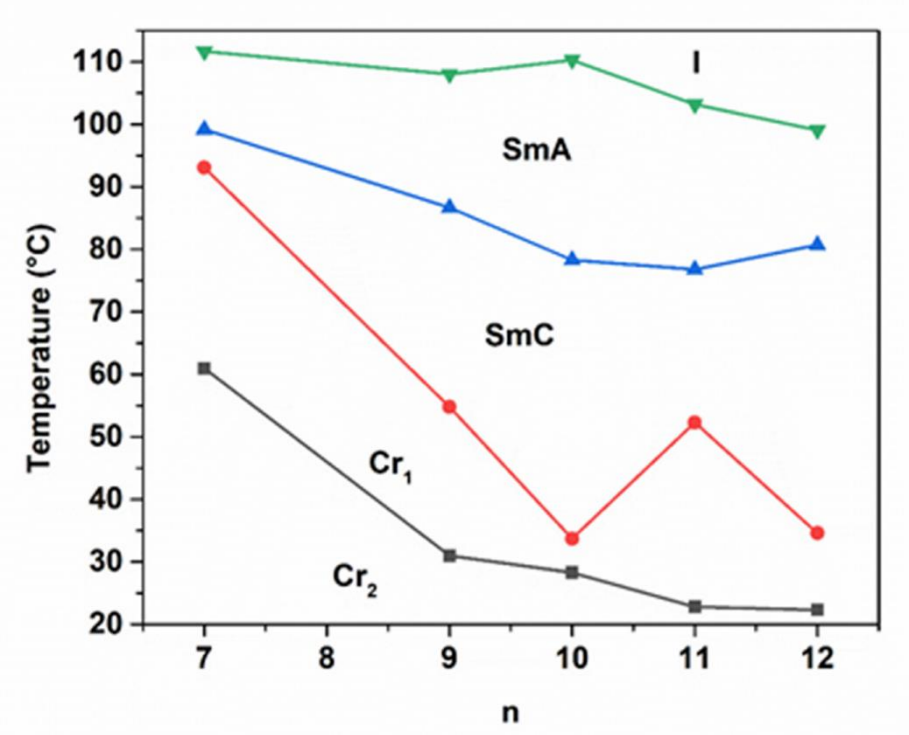

Figure 4. Phase diagram (Temperature–Chain length) (*T*–*n*) for nOBAFF.

Figure 5 illustrates the proposed configuration where the molecules are standing face-to-face with a forced positional order, which favors the layered smectic order as SmC and SmA phases. Although the H- - -F intermolecular interactions have already been exploited by Merkel et al. [32] to stabilize twist bend nematic liquid crystals, this concept is used for the first time to improve the layered structure of SmA and SmC phases.

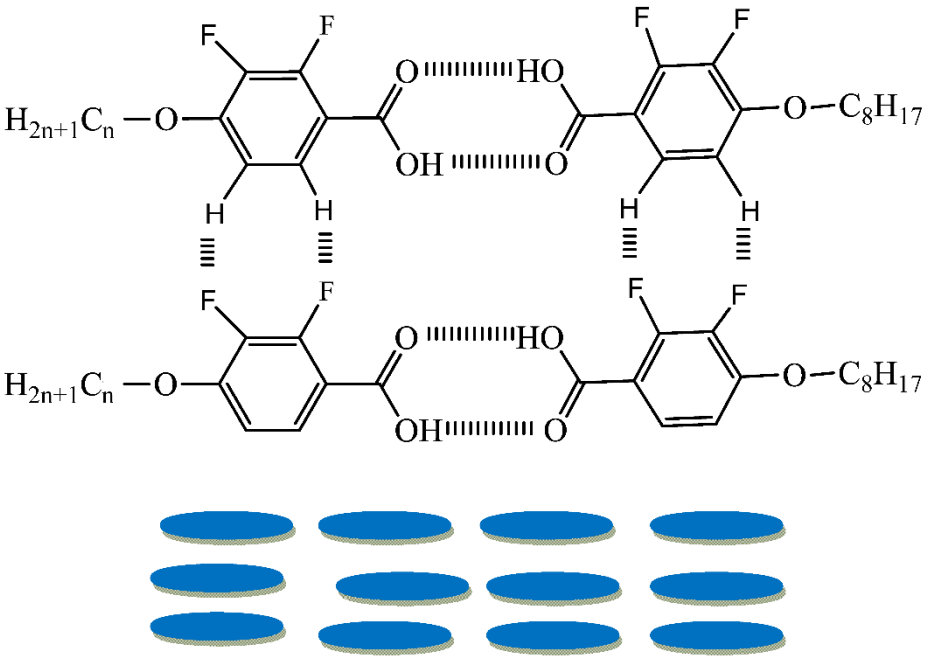

Figure 5. Parallel molecular arrangement induced by intermolecular interactions where the layered smectic order is favored.

IR spectroscopy was used for gaining more information at a molecular level. IR spectra recorded at 20 °C were those of the crystalline phase. Spectra of all mixed nOBAFF/8OBA compounds showed the same features (Figure 6a). They displayed a broad band at 2700–3300 cm^{-1} assigned to the ν(O–H) mode of carboxylic acid groups, a sharp band at 1680 cm^{-1} from ν(C=O) mode, and three sharp bands at 1604, 1513 and 1469 cm^{-1} from the ν(C=C) vibration of the aromatic ring. The band occurring at 1300 cm^{-1} corresponded to C–F stretching vibrations. The sharp band of carbonyl at 1680 cm^{-1} and the absence of absorbance at 3500 cm^{-1} characteristic of the free O–H group confirmed the dimeric association of alkoxybenzoic acids. The wavelength of the carbonyl band is characteristic of the formation of cyclic dimers as shown in Figure 1. The spectra of nOBAFF/8OBA mixtures were compared to those of the pure nOBAFF and 8OBA compounds (Figure 6b and c). All of them showed a single sharp band at 1680 cm^{-1} from the ν(C=O) mode that indicated the predominance of the cyclic dimer form as reported by Martínez-Felipe et al. [11]. Three sharp bands at 1615, 1509 and 1469 cm^{-1} from the ν(C=C) of the aromatic rings were different for the pure compounds and the mixed sample. This feature appeared obvious when the spectrum of the mixture nOBAFF/8OBA was compared to the sum of the spectra of the pure nOBAFF and 8OBA compounds (Figure 7). Thus the sum of the spectra of nOBAFF and 8OBA was generated by normalizing the spectrum of 8OBA using the band at 507 cm^{-1} that was only present in the

spectrum of 8OBA and the spectrum of nOBAFF using the bands of the C–H vibrations at 2800–3000 cm^{-1}. The bands at 1620, 1680, 1420, 1290 and 1080 cm^{-1} were clearly different in the spectra of the mixture and the calculated sum of its components (Figure 7). Firstly, this clearly indicates that the nOBAFF and 8OBA were mixed at a molecular level by co-crystallization because the spectrum of a mixture of crystals of pure nOBAFF and 8OBA would be identical to the calculated sum. Secondly, the largest spectral differences were observed in the spectral region of the C=C vibrations of the aromatic rings, which showed the presence of interactions between nOBAFF and 8OBA molecules at the level the aromatic parts. These spectral differences confirm the hetero-association of the nOBAFF and 8OBA molecules by hydrogen bonding between the carboxylic acid groups. They also provide an experimental clue for the hydrogen bonding interaction between C–H and C–F groups of the aromatic rings (Figure 5).

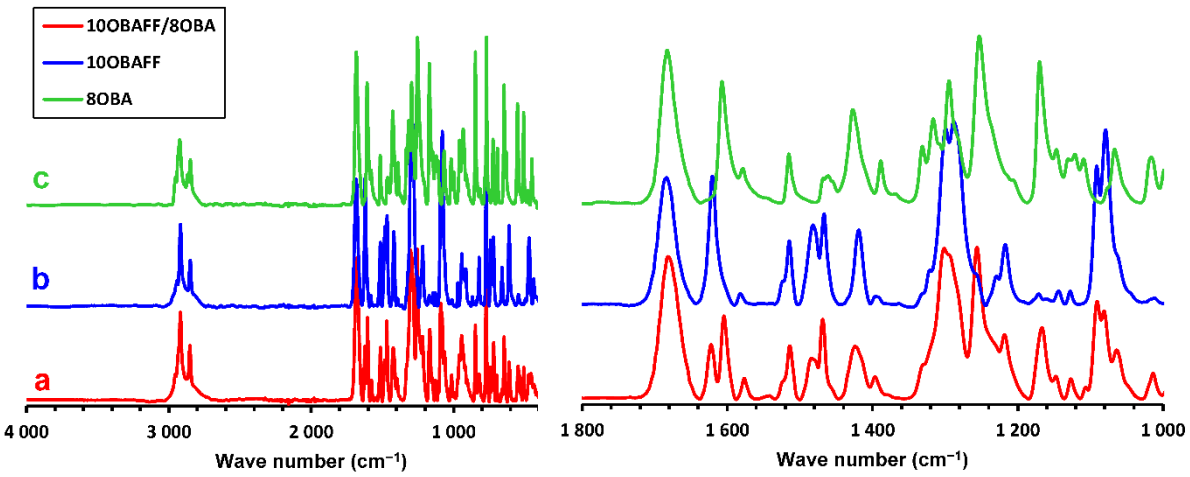

Figure 6. IR spectra of mixed 10OBAFF/8OBA (a) and pure 10OBAF (b) and 8OBA (c). Full scale spectra on the left hand side; expansions between 1000 and 1800 cm^{-1} on the right hand side.

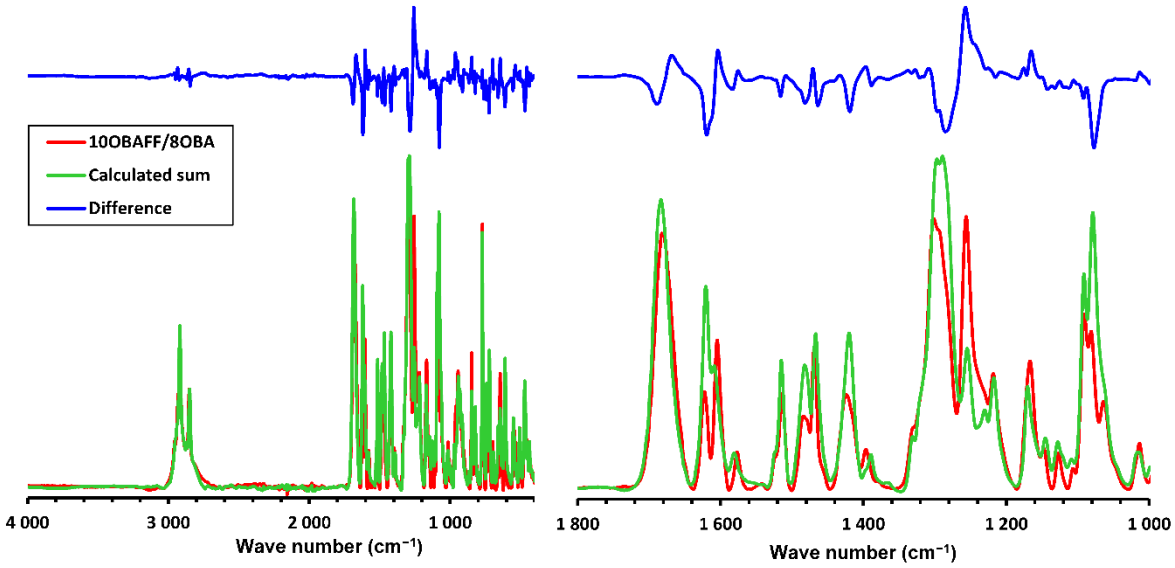

Figure 7. Superimposed IR spectra of mixed 10OBAFF/8OBA and sum of spectra of pure 10OBAFF and 8OBA compounds. The difference between these two spectra in shown in blue on the top. Full-scale spectra on the left hand side; expansions between 1000 and 1800 cm^{-1} on the right hand side.

3.2. Phase behavior of mixed nOBAFF/8OBA

The phase behavior of the studied mixtures of nOBAFF and 8OBA was assessed by DSC, POM and X-ray diffraction experiments as a function of temperature. Figure 8 shows the DSC thermograms of 10OBAFF/8OBA. Four endothermal peaks on heating and four exothermic peaks on cooling indicated the occurrence of three phases between isotropic and crystalline phases for each mixture. These phases were identified from their texture observed by optical microscopy. Indeed, on cooling from the isotropic liquid, the characteristic Schlieren optical texture showing both types of point singularity of the nematic phase was observed (Figure 9a). On further cooling, the smectic phases (SmA) with focal conics and SmC with Schlieren texture were observed as respectively seen in Figures 9b and 9c.

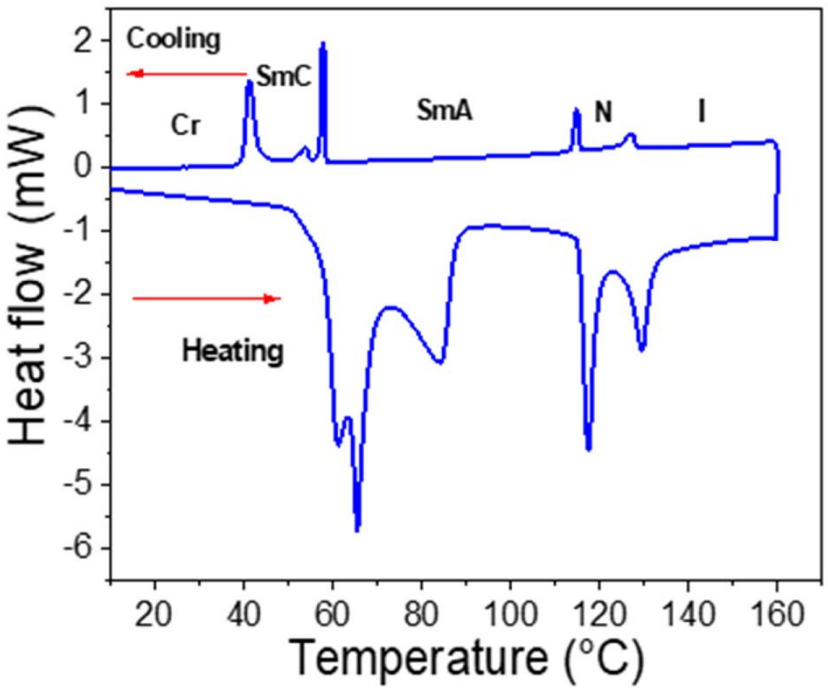

Figure 8. The second heating-cooling DSC trace of 10OBAFF/8OBA.

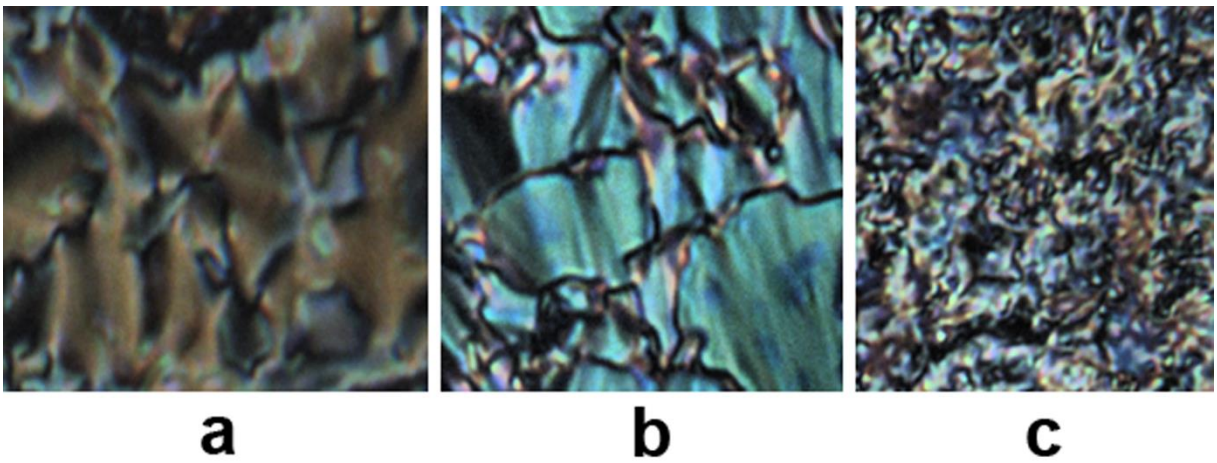

Figure 9. Textures observed by POM on cooling; (a) nematic, (b) SmA and (c) SmC phases for 10OBAFF/8OBA.

The DSC on heating showed a first transition at 57 °C from the Cr phase to the SmC. The SmC phase happened in a narrow temperature range. A transition to the SmA phase started at 62 °C and a DSC signal typical of the coexistence of two phases (SmC + SmA) was observed in the temperature range 62–84 °C. A transition from the SmA phase to the nematic phase was observed at 114 °C. It was followed by a transition to the isotropic phase at 126 °C. The same phase sequence was observed upon cooling. The coexistence of two phases (SmC + SmA) could explain the existence of the large peak on heating and two peaks (strong peak followed by a

small peak) on cooling. The SmA-SmC transition is often second order or very weakly first order, while it is of first order in the present mixture. This means that the character of this transition depends of the materials. In addition, the imperfect mixing would also affect the phase transition; thus nOBAFF/nOBAFF and 8OBA/8OBA with a small fraction could be present. The onsets of formation of the nematic, SmA and SmC phases were at the transition temperatures observed upon cooling. The temperature of formation of the crystalline phase was shifted down with respect to the heating cycle. The SmC phase could be kept in a supercooled state between 57 °C and 44 °C. The SmC phase of 11OBAFF/8OBA and 12OBAFF/8OBA samples was observed by POM only. There was no evidence of a SmA–SmC or SmC–Cr transition in the DSC records of these latter two mixtures.

Table 2. Transition temperatures (°C) and enthalpies ($J \cdot g^{-1}$) of nOBAFF/8OBA observed by DSC and POM experiments upon cooling.

Substances	
9OBAFF/8OBA	Cooling (°C): Cr–(66.5)–SmC–(68.8)–SmA–(115.3)–N–(128.5)–I Enthalpy ($J \cdot g^{-1}$): Cr–(59.8)–SmC–(23.6)–SmA–(10.8)–N–(5.5)–I
10OBAFF/8OBA	Cooling (°C): Cr–(41.1)–SmC–(57.7)–SmA–(114.6)–N–(126.7)–I Enthalpy ($J \cdot g^{-1}$): Cr–(36.7)–SmC–(22.9)–SmA–(9.9)–N–(6.0)–I
11OBAFF/8OBA	Cooling (°C): Cr–(21.7)–SmC–(54.83)–SmA–(114.1)–N–(125.8)–I Enthalpy ($J \cdot g^{-1}$): Cr–(1.8)–SmC–(50.6)–SmA–(9.6)–N–(6.3)–I
12OBAFF/8OBA	Cooling (°C): Cr–(20)–SmC–(42.9)–SmA–(107.8)–N–(115.1)–I Enthalpy ($J \cdot g^{-1}$): Cr–(0.1)–SmC–(55.3)–SmA–(5.1)–N–(2.0)–I

The X-ray diffraction powder patterns of the different phases confirmed the observations by POM. The isotropic phase showed a characteristic Debye–Scherrer ring corresponding to a disordered organization of molecules in their molten state. The nematic phase was oriented with its director perpendicular to the wall of the glass capillary. This orientation possibly came from the hydrogen bonds between the carboxylic acid groups of the 10OBAFF and 8OBA molecules and the Si–OH groups at the surface of the glass. The diffraction pattern of the SmA phase misses the Bragg peak of the long period of the lamellar order because this peak is located at smaller angles than the minimum angle of the diffraction set-up. Transition to the SmA phase kept the orientation of the director, though the more random angular distribution of the scattered

X-ray light revealed a slight disorientation. Finally, the crystalline phase showed the characteristic pattern of a polycrystalline powder with well-defined Bragg reflexions.

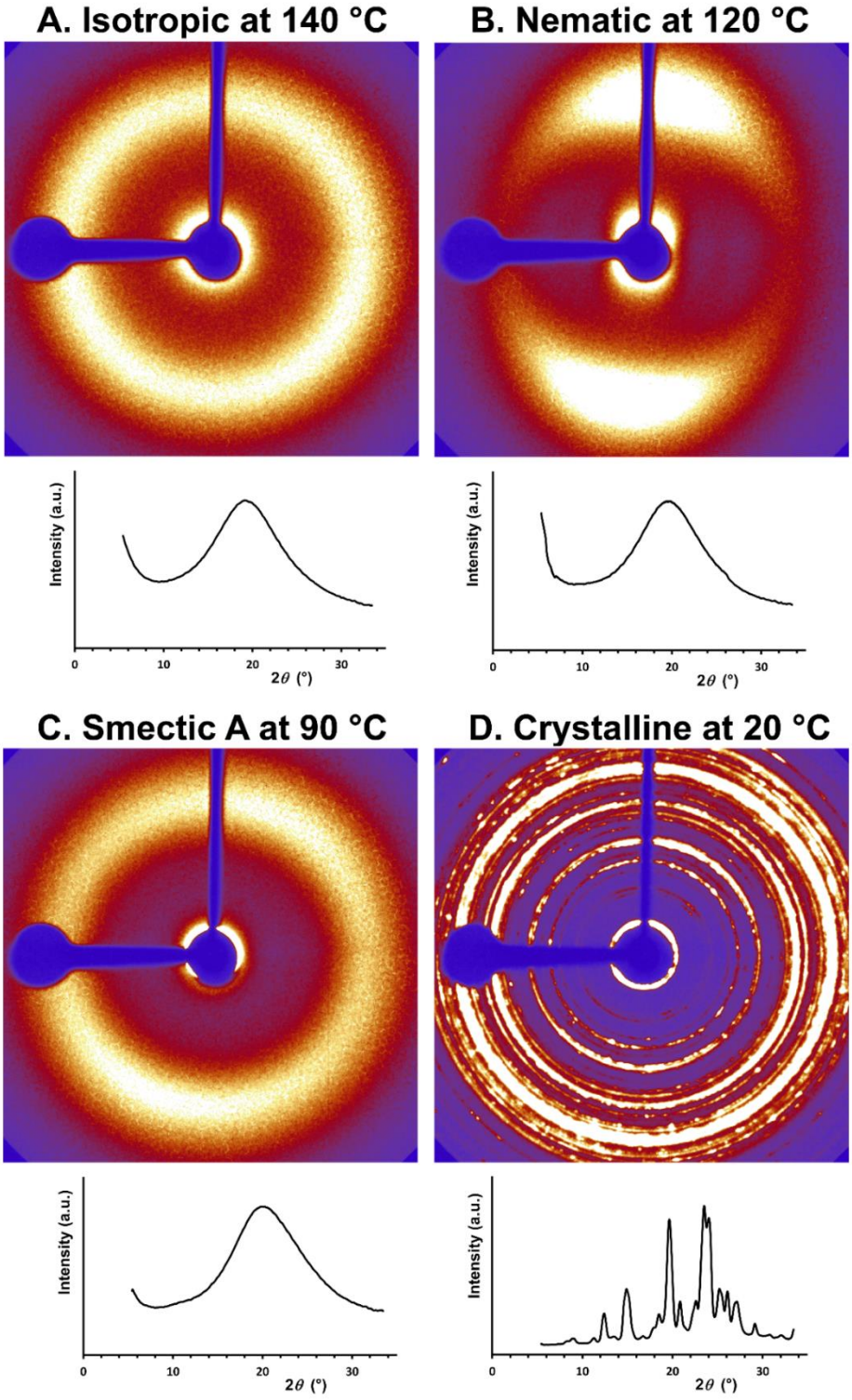

Figure 10. Debye–Scherrer powder patterns of X-ray diffraction subsequent phases upon cooling; (A) isotropic at 140 °C, (B) nematic at 120 °C, (C) SmA at 90 °C, and (D) crystalline at 20 °C for 10OBAFF/8OBA. Both the 2D picture of the detector and the 1D radial-averaged powder pattern are shown.

As seen from the phase diagrams of the mixtures (Figure 11), the clearing temperature ($T_{N–I}$) slightly decreased with the chain length (n), while the crystallization temperature ($T_{Cr–SmC}$) decreased more drastically than the clearing point. In addition, the stability of nematic phase remained constant, while the stability of the SmC increased with increasing n. It increased from ΔT = 4.2 °C for 7OBAFF/8OBA to ΔT = 18.4 °C for 12OBAFF/8OBA. The widening of the SmC phase was at the expense of the low-temperature crystalline phase. The long flexible chain stabilizes the liquid phases against the crystalline phase with the alkyl chains perfectly ordered in their all-trans configuration. This behavior is consistent with the results on hydrogen-bonded liquid crystals reported by Saccone et al. [33], which reveal that increasing chain length enhances the stability of the assemblies of smectic phases and lowers both the clearing and melting points. In addition, our previous work disclosed that the monofluorinated compounds nOBAF displayed nematic and SmC phases and that $T_{I–N}$ decreased as n increased [19]. However, the melting temperature increased with respect to the length of the alkyl chain. Parra et al. [34] disclosed a decrease of both clearing and melting temperatures with increasing the chain length for a series of liquid crystalline amides incorporating pyridine and thiadiazole rings. For the present complexes, the melting temperature (T_{Cr-SmC}) was shifted from 86 °C for 9OBAFF/8OBA to 61 °C for the other complexes (SI file).

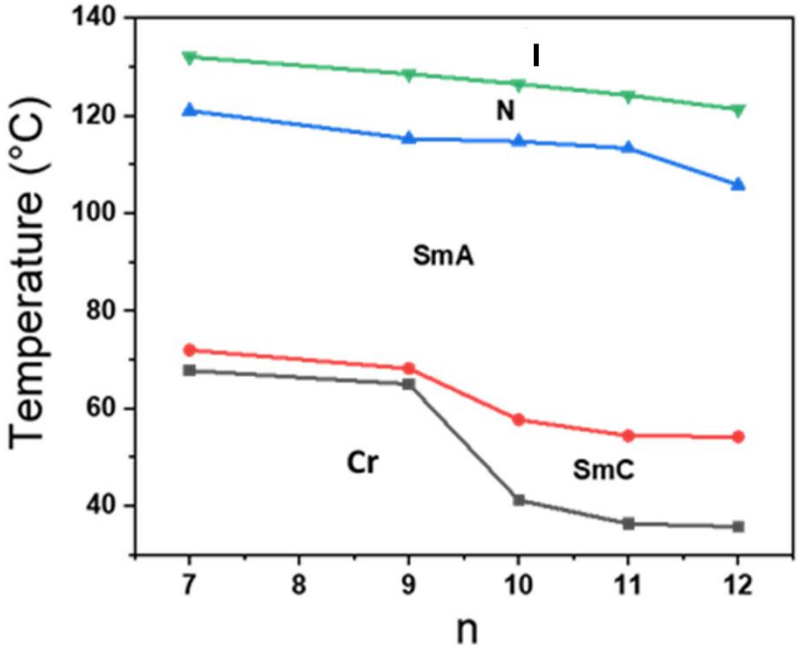

Figure 11. Phase diagram (Temperature–Chain length) (T–n) for nOBAFF/8OBA complexes inferred from POM observations upon cooling.

The most important difference between the phase diagrams of the obtained complexes and the individual compounds is the presence of the nematic phase in the complexes. However, the temperature range of nematic phase in these complexes is less than that in pure 8OBA (20 °C) [21]. We will nevertheless show that the physical properties for these mixtures are improved compared to that of pure 8OBA.

3.3. Dielectric properties

Figure 12 presents the frequency dependence of real and imaginary parts of the dielectric constant at several temperatures. Two distinct relaxation modes are observed. At low frequencies, the ionic contribution to dielectric constant is clearly seen in the 1–100 Hz range. The maximum of ε'' is only visible in the observed frequency range at 124 °C; it is at lower frequency for lower temperatures. Such relaxation may be attributed to the space charge, which is suppressed under electric field. The second relaxation at 1.2 MHz is related to molecular rotation around their long axis. It slightly decreases with respect to the temperature. The two mentioned processes of dielectric relaxation have been observed in [35,36]. The same data collected for the pure components 10OBAFF and 8OBA showed the same features. Their relaxation frequencies as a function of temperature are given in Figure 13, together with that of the 10OBAFF/8OBA mixture.

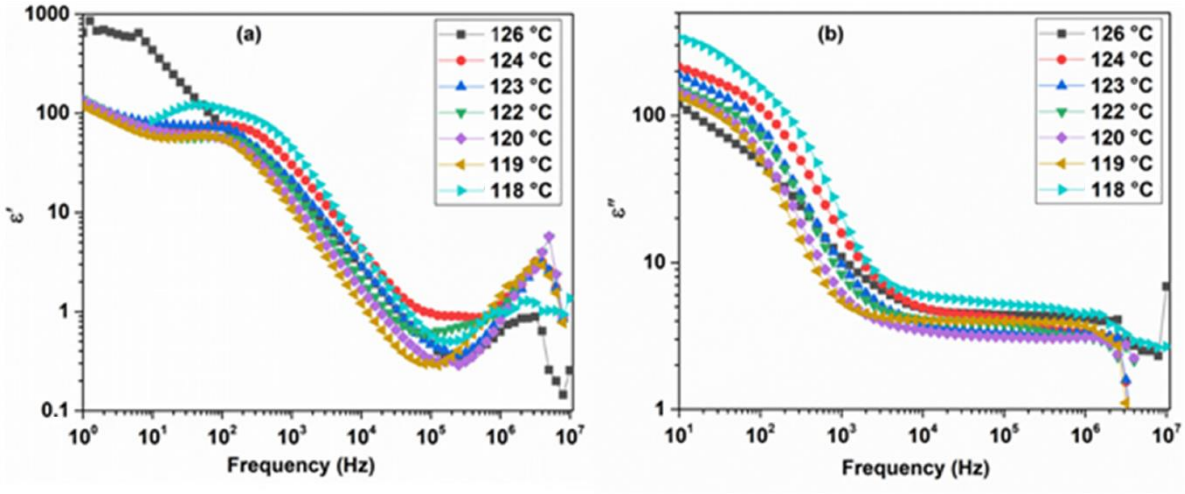

Figure 12. Frequency dependence of ε' (a) and ε'' (b) for 10OBAFF/8OBA at several temperatures.

Figure 13 presents the relaxation frequency as a function of the inverse temperature for the mixture 10OBAF/8OBA and the individual compounds. All the curves present the Arrhenius behavior:

$$f_R = f_0 e^{\frac{-E_a}{k_B T}} \quad (1)$$

where E_a is the activation energy and k_B is Boltzmann constant. It was found that E_a is 0.2 eV, 1,5 eV and 0.8 eV for 8OBA, 10OBAFF and 10OBAFF/8OBA, respectively. The highest value of E_a for the 10OBAFF can be explained by the H…F intermolecular interactions (Figure 5).

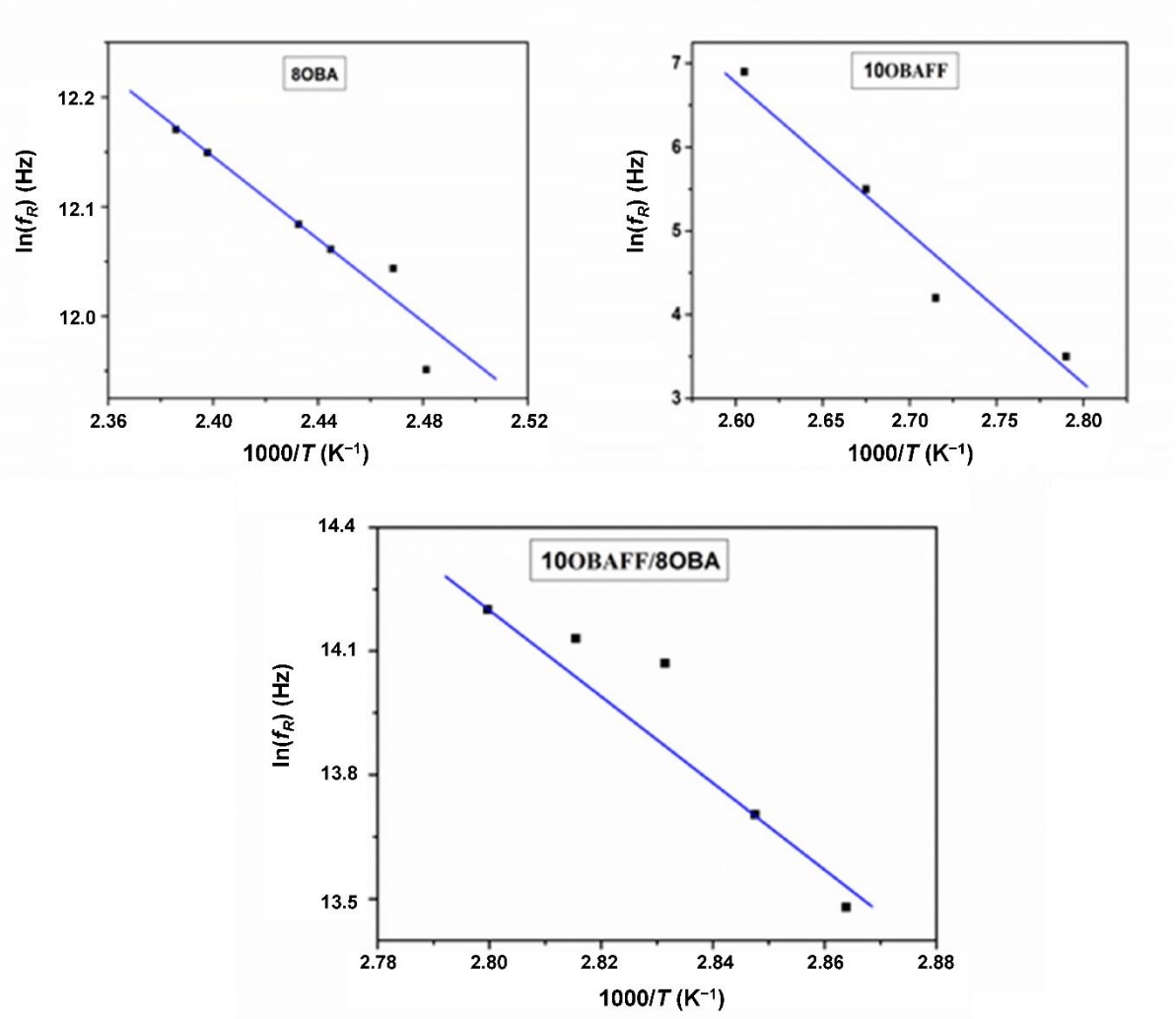

Figure 13. Plots of the temperature dependence of the relaxation frequency for 8OBA, 10OBAFF and 10OBAFF/8OBA compounds.

The variation of dielectric anisotropy ($\Delta\varepsilon$) at 10 kHz with the temperature is shown in Figure 14. The dielectric anisotropy is positive in all the mixtures and exhibits a typical behavior, that is, $\Delta\varepsilon$ increases with decreasing temperature. At lower temperature of nematic phase, the dielectric anisotropy is larger for the short chain length. For example, it decreases from 1.7 for

7OBAF/8OBA to 1.3 for 10OBAF/8OBA. Similar behavior has been observed in other nematic LCs; for example, $\Delta\varepsilon$ of 5CB ($\Delta\varepsilon$ = 12) [37] is higher than that of 8CB ($\Delta\varepsilon$ = 8.5) [38,39]. Moreover, the present values are slightly higher than that of pure 8OBA ($\Delta\varepsilon$ = 0.9) and pure 8OBAF ($\Delta\varepsilon$ = 0.7) [21], whereas it is much lower than that of the well-known nematic 5CB.

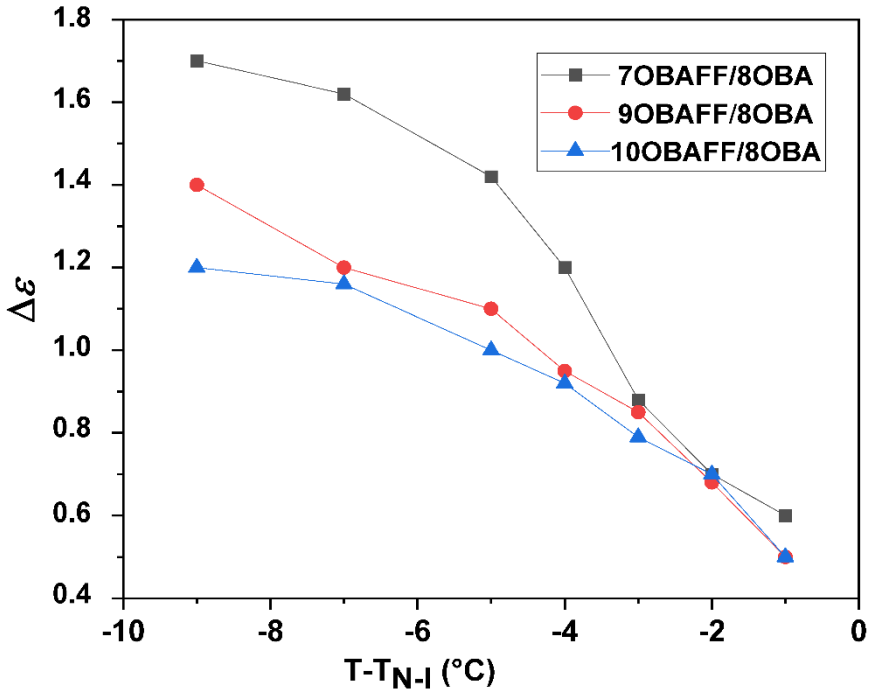

Figure 14. Variation of dielectric anisotropy as function of temperature for nOBAFF/8OBA (n = 7, 9 and 10).

3.4. Electro-optic properties

Threshold voltages of the Fréedericksz transition (V_{th}) and response times (τ) for flipping were investigated for nOBAFF/8OBA (n = 7, 9 and 10) mixtures in order to compare them with that of pure 8OBA on one hand and show the effect of chain length on these behaviors on other hand. The threshold variations with respect to temperature for nOBAFF/8OBA (n = 7, 9 and 10) mixtures are given in Figure 15. V_{th} decreases with increasing temperature for all samples. It decreases from 6.8 V for 7OBAFF/8OBA to 5.4 V for 10OBAFF/8OBA at $T - T_{IN} = -9$ °C. These values are lower than that of pure 8OBA [21].

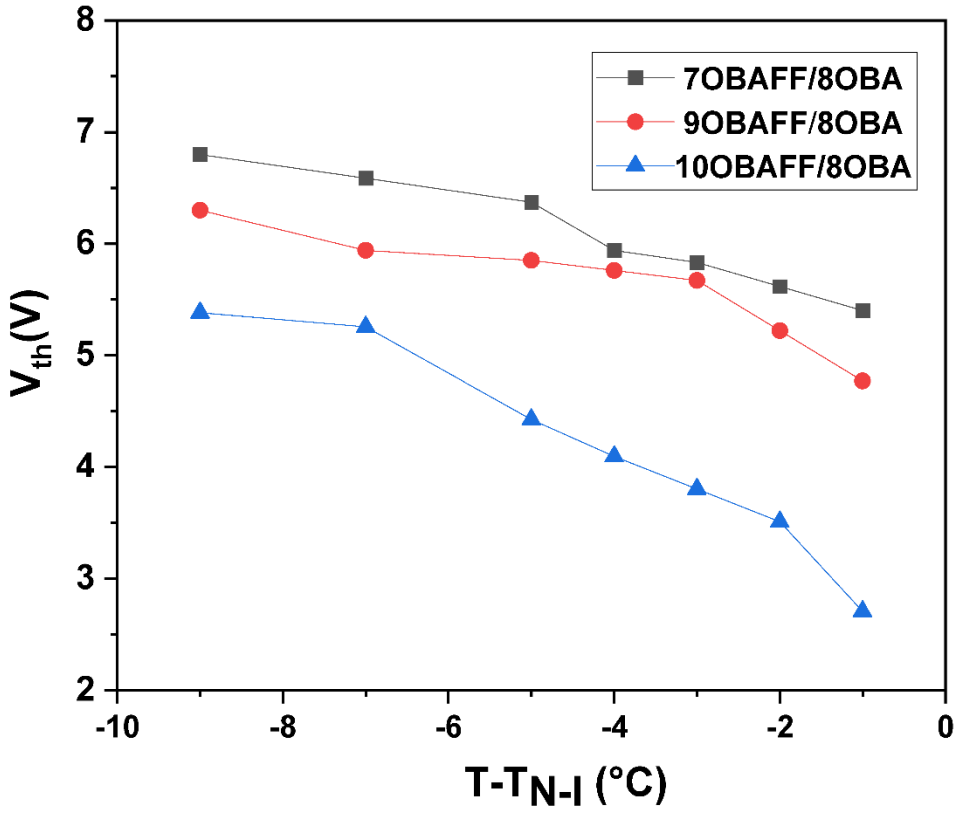

Figure 15. Temperature dependence of threshold voltages for nOBAFF/8OBA (*n* = 7, 9 and 10).

The response time (τ), defined as the time taken by the molecules between two their stable states (ON to OFF state), decreases for both mixtures with increasing temperature near the N–I transition and follows a first-order phase transition behavior (Figure 16). It is worth mentioning that the decrease of clearing temperature, threshold and response time with increasing chain length suggests that the order parameter decreases with respect to *n*, which can be explained by the free space provided by longer chain length; therefore, molecular density tends to decrease with an increase in the alkyl chain length. This is in good agreement with previous observations for nOBAF [19]. In addition, V_{th} and τ for the present complexes are much lower than that of 8OBA [21]. This behavior can be explained by the high polarity of these complexes having a non-symmetric dimer shape compared to symmetrical dimer of 8OBA. Such features of the response time and threshold are significant improvements compared to the characteristics of pure 8OBA. The enhancement in the phase stability compared to that for pure nOBAFF is another benefit of mixing nOBAFF and 8OBA.

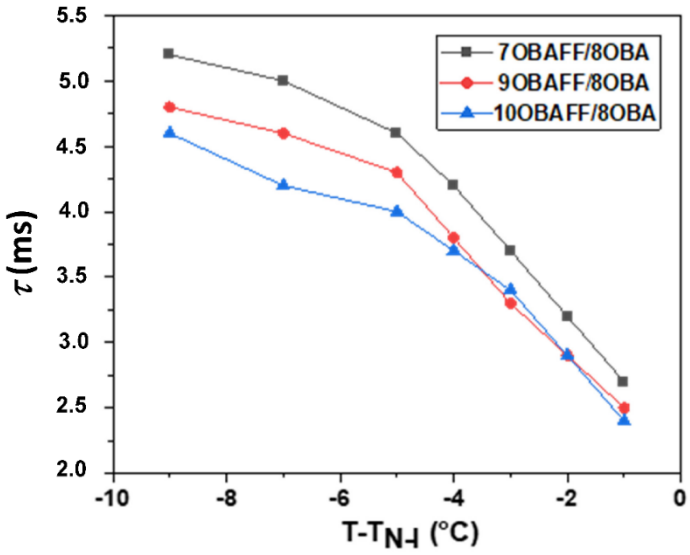

Figure 16. Temperature dependence of response time for nOBAFF/8OBA (n = 7, 9 and 10).

3.5. Viscoelastic properties

The $V_{th}(T)$ and $\tau(T)$ properties are related to the viscoelastic behavior. The elastic constant (K_{11}) and rotational viscosity (γ) are calculated using the following expressions [39,40]:

$$K_{11} = \frac{\varepsilon_0 \, \Delta\varepsilon \, V_{th}^2}{\pi^2} \tag{2}$$

$$\gamma = \frac{\tau \, K_{11} \, \pi^2}{d^2} \tag{3}$$

The splay elastic K_{11} decreases with increasing the temperature as seen in Figure 17. Moreover, as expected, K_{11} deceases with increasing chain length. According to the Eq. 2, a decrease of V_{th} should cause a decrease of K_{11}. At high temperatures near the I–N transition, K_{11} of all materials are of comparable magnitude, while at lower temperature K_{11} decreases rapidly with increasing terminal alkoxy chain length. Yildiz et al. [41] reported similar temperature variation of K_{11} in the entire nematic domain of 8CB. The values of K_{11} for 8CB are lower than that in the present complexes.

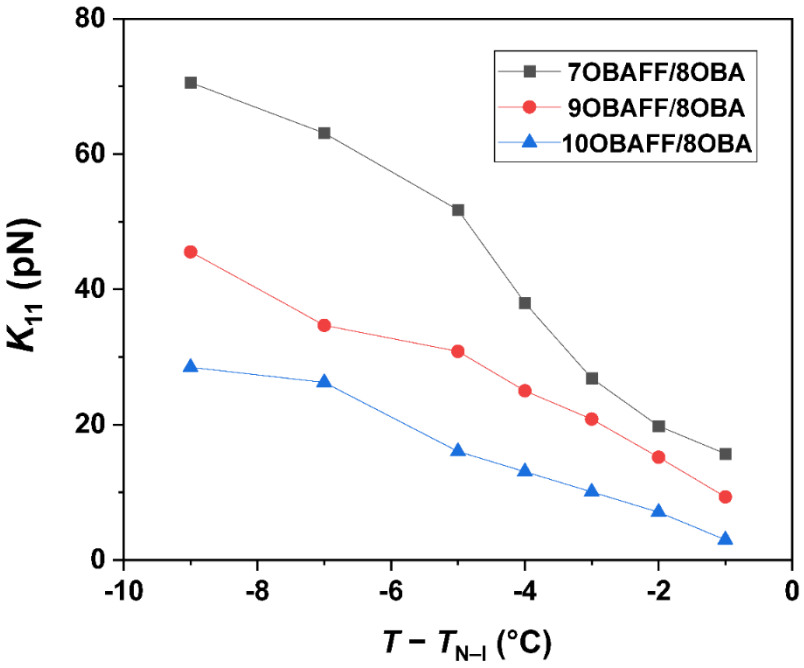

Figure 17. Variation of the splay elastic constant as function of temperature for 7OBAFF/8OBA, 9OBAFF/8OBA and 10OBAFF/8OBA.

The dependence of the rotational viscosity, γ, on temperature for the mixture is shown in Figure 18. γ decreased with respect to temperature. In addition, the highest value of γ was obtained for the short chain length. The alkoxy chain length dependence of the rotational viscosity showed that γ strongly depended to the molecular density. This behavior has been observed in several instances suggesting that the longer chain length liquid crystal molecules reduces the molecular density [2,19,41]. Moreover, this result provides better insight into the dependence of the response time on the alkyl chain length.

The rotational viscosity quickly decreased upon increasing the alkoxy chain length. K_{11} and γ for 7OBAFF/8OBA were much higher than other complexes and quickly varied with the temperature in the lower temperature range of the nematic phase. Interestingly, γ of the present mixtures were much lower than that of the individual compounds 8OBA and other calamitic nematic LCs, for example 5CB [37] and 8CB [39].

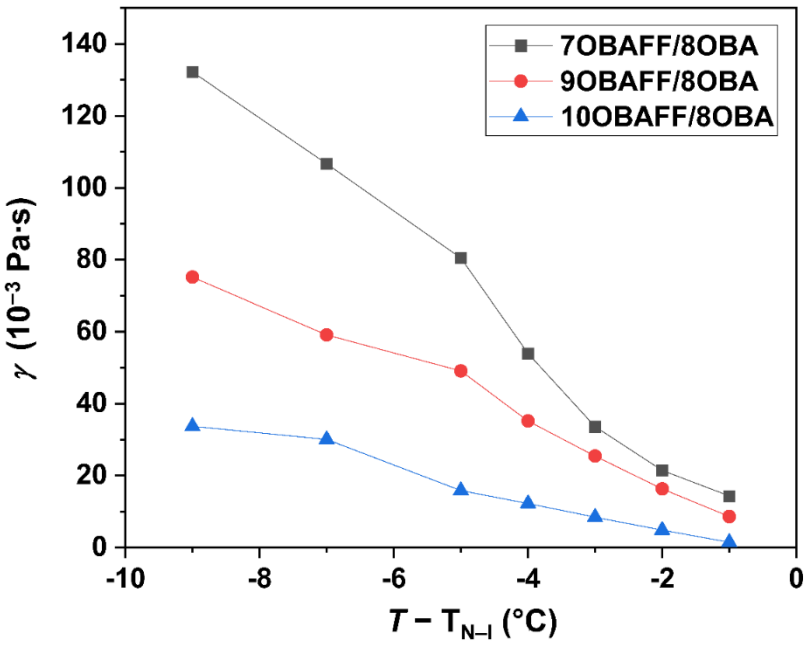

Figure 18. Variation the rotational viscosity with respect to temperature for 7OBAFF/8OBA, 9OBAFF/8OBA and 10OBAFF/8OBA.

4. Conclusion

Two new series of fluorinated HBLCs were synthesized and characterized by NMR and IR spectroscopic analyses. The first ones are the pure nOBAFF compounds, and the second ones are the 1:1 hydrogen-bonded supramolecular complexes between nOBAFF and 8OBA. The thermodynamic properties of these complexes were investigated by DSC, POM and XRD measurements. nOBAFF compounds exhibit SmA and SmC phases and do not form a nematic phase. Strong intermolecular hydrogen bonds between H and F atoms of neighboring molecules provide a rationale to the phase behavior. The mixtures nOBAFF/8OBA display nematic, SmA and SmC phases. Mixing 8OBA with nOBAFF stabilizes the nematic phase. The effect of the length of the alkoxy chain on the thermal stability is clearly observed. The decrements of clearing temperature, threshold and response time are attributed to a reduction of the order parameter when the chain length increases. Mixing a difluorinated compound with 8OBA allows the formation of a nematic phase containing highly fluorinated molecules that bring about interesting electro-optical properties. Such features of the nematic phase of mixed nOBAFF/8OBA are definite benefits in the framework of possible applications to liquid crystal displays.

Funding. The Deanship of Scientific Research at Imam Mohammad Ibn Saud Islamic.

Acknowledgments. The authors extend their appreciation to the Deanship of Scientific Research at Imam Mohammad Ibn Saud Islamic University for funding this work through Research Group no. RG-21-09-67.

Conflicts of Interest. The authors declare no conflict of interest.

References

[1] C.M. Paleos, D. Tsiourvas, Supramolecular hydrogen-bonded liquid crystals, Liquid Cryst. 28 (2001) 1127–1161, doi:10.1080/02678290110039516.

[2] P. Bhagavath, S. Mahabaleshwara, S.G. Bhat, D.M. Potukuchi, P. Shetty, S. Maddasani, Influence of polar substituents and flexible chain length on mesomorphism in non-mesogenic linear hydrogen bonded complexes, J. Mol. Liquids 336 (2021) 116313, doi:10.1016/j.molliq.2021.116313.

[3] F.S. Alamro, O.A. Alhaddad, M.M. Naoum, H.A. Ahmed, Polymorphic phases of supramolecular liquid crystal complexes laterally substituted with chlorine, Polymers 13 (2021) 4292, doi:10.3390/polym13244292.

[4] S.J.D. Lugger, S.J.A. Houben, Y. Foelen, M.G. Debije, A.P.H.J. Schenning, D.J. Mulder, Hydrogen-bonded supramolecular liquid crystal polymers: Smart materials with stimuli-responsive, self-healing, and recyclable properties, Chem. Rev. 122 (2022) 4946–4975, doi:10.1021/acs.chemrev.1c00330.

[5] G.W. Gray, B. Jones, Influence of substituents on the mesomorphism of *p*-*n*-alkoxybenzoic and 6-*n*-alkoxy-2-naphthoic acids, Nature 170 (1952) 451–452, doi:10.1038/170451a0.

[6] N. Pongali Sathya Prabu, M.L.N. Madhu Mohan, Characterization of a new smectic ordering in supramolecular hydrogen bonded liquid crystals by X-ray, optical and dielectric studies, J. Mol. Liquids 182 (2013) 79–90, doi:10.1016/j.molliq.2013.03.014.

[7] M. Okumuş, Investigation of thermal and optical properties of some quartet mixed hydrogen-bonded liquid crystals, Int. J. Mod. Phys. B 31 (2017) 1750224, doi:10.1142/S0217979217502241.

[8] M. Fouzai, R. Hamdi, S. Ghrab, T. Soltani, A. Ionescu, T. Othman, Properties of binary mixtures derived from hydrogen bonded liquid crystals, J. Mol. Liquids 249 (2018) 1279–1286, doi:10.1016/j.molliq.2017.11.128.

[9] H.A. Ahmed, M. Hagar, M. Alaasar, M. Naoum, Wide nematic phases induced by hydrogen-bonding, Liquid Cryst. 46 (2019) 550–559, doi:10.1080/02678292.2018.1512664.

[10] M. Okumuş, Synthesis and characterization of hydrogen bonded liquid crystal complexes by 4-octyloxy benzoic acid and some dicarboxylic acids, J. Mol. Liquids 266 (2018) 529–534, doi:10.1016/j.molliq.2018.06.111.

[11] A. Martínez-Felipe, A.G. Cook, M.J. Wallage, C.T. Imrie, Hydrogen bonding and liquid crystallinity of low molar mass and polymeric mesogens containing benzoic acids: a variable temperature Fourier transform infrared spectroscopic study, Phase Trans. 87 (2014) 1191–1210, doi:10.1080/01411594.2014.900556.

[12] B. Meddeb, A. Gesmi, N. Ben Hamadi, T. Soltani, Enhancement of thermal, dielectric and electro-optical properties of fluoro hydrogen-bonded liquid crystals, Liquid Cryst. 48 (2021) 1175–1185, doi:10.1080/02678292.2020.1850895.

[13] A.V.N. Ashok Kumar, B. Sridevi, M. Srinivasulu, P.V. Chalapathi, D.M. Potukuchi, Inductive effect for the phase stability in hydrogen bonded liquid crystals, x-(p/m)BA:9OBAs, Liquid Cryst. 41 (2014) 184–196, doi:10.1080/02678292.2013.846425.

[14] T. Kato, J.M.J. Fréchet, A new approach to mesophase stabilization through hydrogen bonding molecular interactions in binary mixtures, J. Am. Chem. Soc. 111 (2002) 8533–8534, doi:10.1021/ja00204a044.

[15] Y. Arakawa, Y. Sasaki, H. Tsuji, Supramolecular hydrogen-bonded liquid crystals based on 4-*n*-alkylthiobenzoic acids and 4,4′-bipyridine: Their mesomorphic behavior with comparative study including alkyl and alkoxy counterparts, J. Mol. Liquids 280 (2019) 153–159, doi:10.1016/j.molliq.2019.01.119.

[16] R. Walker, D. Pociecha, J.P. Abberley, A. Martinez-Felipe, D.A. Paterson, E. Forsyth, G.B. Lawrence, P.A. Henderson, J.M.D. Storey, E. Gorecka, C.T. Imrie, Spontaneous chirality through mixing achiral components: a twist-bend nematic phase driven by hydrogen-bonding between unlike components, Chem. Commun. 54 (2018) 3383–3386, doi:10.1039/C8CC00525G.

[17] H.A. Ahmed, M. Hagar, A. Aljuhani, Mesophase behavior of new linear supramolecular hydrogen-bonding complexes, RSC Adv. 8 (2018) 34937–34946, doi:10.1039/C8RA07692H.

[18] R. Walker, D. Pociecha, C.A. Crawford, J. Storey, E. Górecka, C. Imrie, Hydrogen bonding and the design of twist-bend nematogens, J. Mol. Liquids 303 (2020) 112630, doi:10.1016/j.molliq.2020.112630.

[19] T. Missaoui, I. Ben Amor, T. Soltani, H. Ben Ouada, E. Jeanneau, Y. Chevalier, Dielectric and electro-optic properties of cybotactic nematic phase in hydrogen-bonded liquid crystals, J. Mol. Liquids 304 (2020) 112726, doi:10.1016/j.molliq.2020.112726.

[20] H. Nishikawa, K. Shiroshita, H. Higuchi, Y. Okumura, Y. Haseba, S.-I. Yamamoto, K. Sago, H. Kikuchi, A fluid liquid-crystal material with highly polar order, Adv. Mater. 29 (2017) 1702354, doi:10.1002/adma.201702354.

[21] M. Fouzai, A. Guesmi, N.B. Hamadi, T. Soltani, Fluoro-substitution in hydrogen bonding liquid crystal benzoic acid: dielectric, electro-optic and optical proprieties and inducing polar nematic phase, Liquid Cryst. 47 (2020) 777–784, doi:10.1080/02678292.2019.1679900.

[22] R.J. Mandle, S.J. Cowling, J.W. Goodby, Rational design of rod-like liquid crystals exhibiting two nematic phases, Chem. Eur. J. 23 (2017) 14554–14562, doi:10.1002/chem.201702742.

[23] M. Spengler, R.Y. Dong, C.A. Michal, M. Pfletscher, M. Giese, Fluorination of supramolecular liquid crystals – tuning tool and analytical probe, J. Mater. Chem. C. 5 (2017) 2235–2239, doi:10.1039/C6TC05472B.7.

[24] M. Iliș, M. Micutz, I. Pasuk, T. Staicu, V. Cîrcu, Synthesis and liquid crystalline properties of novel fluorinated N-benzoyl thiourea compounds. Effect of perfluoroalkyl chains on the thermal behavior and smectic phases stability, J. Fluorine Chem. 204 (2017) 84–89, doi:10.1016/j.jfluchem.2017.10.008.

[25] R. Hamdi, Synthesis and physicochemical studies of double fluorinated hydrogen-bonded liquid crystals (n-OBAFF), J. Mol. Liquids 349 (2022) 118201, doi:10.1016/j.molliq.2021.118201.

[26] D. Vorländer, Über die Natur der Kohlenstoffketten in kristallin-flüssigen Substanzen. Z. Phys. Chem. 126 (1927) 449–472, doi:10.1515/zpch-1927-12629.

[27] A. Jakli, Odd-even effects in liquid crystals, Liquid Cryst. 49 (2022) 1010–1019, doi:10.1080/02678292.2021.2000054.

[28] C.D. Mukherjee, T.R. Bose, D. Ghosh, M.K. Roy, M. Saha, On the even odd effect in smectic-nematic transitions, Mol. Cryst. Liq. Cryst. 124 (1985) 139–147, doi:10.1080/00268948508079472.

[29] Y. Yamamura, R. Tsuchiya, S. Fujimura, M. Hishida, K. Saito, Odd–even effect on nematic SmA_d phase boundary and SmA_d structure in homologous binary systems of cyanobiphenyl mesogens: 4-alkyl-4'-cyanobiphenyl (*n*CB) and 4-alkoxy-4'-cyanobiphenyl (*n*OCB), J. Phys. Chem. B 121 (2017) 1438−1447, doi:10.1021/acs.jpcb.6b12977.

[30] M. Takahashi, S. Mita, S. Kondo, On the even-odd effect of volume changes at I/N and N/SmA transitions, Mol. Cryst. Liq. Cryst. 147 (1987) 99–105, doi:10.1080/00268948708084627.

[31] J. Jadżyn, G. Czechowski, N.T. Shonova, Odd-even effects in the dielectric properties of nematics 4-(trans-4′-*n*-alkylcyclohexyl)isothiocyanatobenzenes. Liquid Cryst. 3 (1988) 1637–1641, doi:10.1080/02678298808086626.

[32] K. Merkel, B. Loska, C. Welch, G. H. Mehl, A. Kocot, The role of intermolecular interactions in stabilizing the structure of the nematic twist-bend phase, RSC Adv. 11 (2021) 2917–2925, doi:10.1039/D0RA10481G.

[33] M. Saccone, M. Pfletscher, S. Kather, C. Wölper, C. Daniliuc, M. Mezger, M. Giese, Improving the mesomorphic behaviour of supramolecular liquid crystals by resonance-assisted hydrogen bonding, J. Mater. Chem. C 7 (2019) 8643–8648, doi:10.1039/C9TC02787D.

[34] M. Parra, J. Alderete, C. Zúñiga, S. Hernández, Synthesis, mesomorphic properties and structural study by semi-empirical calculations of amides containing the 1,3,4-thiadiazole unit, Liquid Cryst. 29 (2002) 647–652, doi:10.1080/02678290210126068.

[35] L.F. Chiriac, P.C. Ganea, D.M. Maximean, I. Pasuk, V. Cîrcu, Synthesis and thermal, emission and dielectric properties of liquid crystalline Eu(III), Sm(III) and Tb(III) complexes based on mesogenic 4-pyridone ligands functionalized with cyanobiphenyl groups, J. Mol. Liquids 290 (2019) 111184, doi:10.1016/j.molliq.2019.111184.

[36] D.M. Maximean, V. Cîrcu, C.P. Ganea, Dielectric properties of a bisimidazolium salt with dodecyl sulfate anion doped with carbon nanotubes, Beilstein J. Nanotechnol. 9 (2018) 164–174, doi:10.3762/bjnano.9.19.

[37] H. Ayeb, M. Derbali, A. Mouhli, T. Soltani, F. Jomni, J. Fresnais, E. Lacaze, Viscoelastic and dielectric properties of 5CB nematic liquid crystal doped by magnetic and

nonmagnetic nanoparticles, Phys. Rev. E 102 (2020) 052703, doi:10.1103/PhysRevE.102.052703.

[38] R. Nasri, T. Missaoui, A. Hbibi, T. Soltani, Enhanced dielectric properties of Nematic liquid crystal doped with ferroelectric nanoparticles, Liquid Cryst. 48 (2021) 1429–1437, doi:10.1080/02678292.2021.1876934.

[39] S. Yildiz, I. Koseoglu, M.C. Cetinkaya, Temperature-dependent electro-optical and elastic properties of carbon nanotube doped polar smectogen octylcyanobiphenyl, J. Mol. Liquids 209 (2015) 729–737, doi:10.1016/j.molliq.2015.06.043.

[40] M. Derbali, A. Guesmi, N.B. Hamadi, T. Soltani, Dielectric, electrooptic and viscoelastic properties in cybotactic nematic phase doped with ferroelectric nanoparticles, J. Mol. Liquids 319 (2020) 113768, doi:10.1016/j.molliq.2020.113768.

[41] J.-W. Lee, J.-I. Jin, M.F. Achard, F. Hardouin, Cholesterol-based hydrogen-bonded liquid crystals, Liquid Cryst. 30 (2003) 1193–1199, doi:10.1080/02678290310001599233.

Supporting Information

Synthesis, thermal, dielectric and electro-optic properties of new series of fluorinated hydrogen-bonded liquid crystals

Mouna Derbali[a], Taoufik Soltani[a*], Ahlem Guesmi[b], Naoufel Ben Hamadi[b], Erwann Jeanneau[c], Yves Chevalier[d*]

[a] Université de Tunis El Manar, Faculté des Sciences de Tunis, LR99ES16 Laboratoire Physique de la Matière Molle et de la Modélisation Électromagnétique, 2092 Tunis, Tunisia.
[b] Chemistry Department, College of Science, IMSIU (Imam Mohammad Ibn Saud Islamic University), Riyadh, Kingdom of Saudi Arabia.
[c] Université Claude Bernard Lyon 1, Centre de Diffractométrie Henri Longchambon, 69622 Villeurbanne, France.
[d] Université Claude Bernard Lyon 1, Laboratoire d'Automatique, de Génie des Procédés et de Génie Pharmaceutique, LAGEPP, CNRS UMR 5007, 43 bd 11 Novembre, 69622 Villeurbanne Cedex, France.

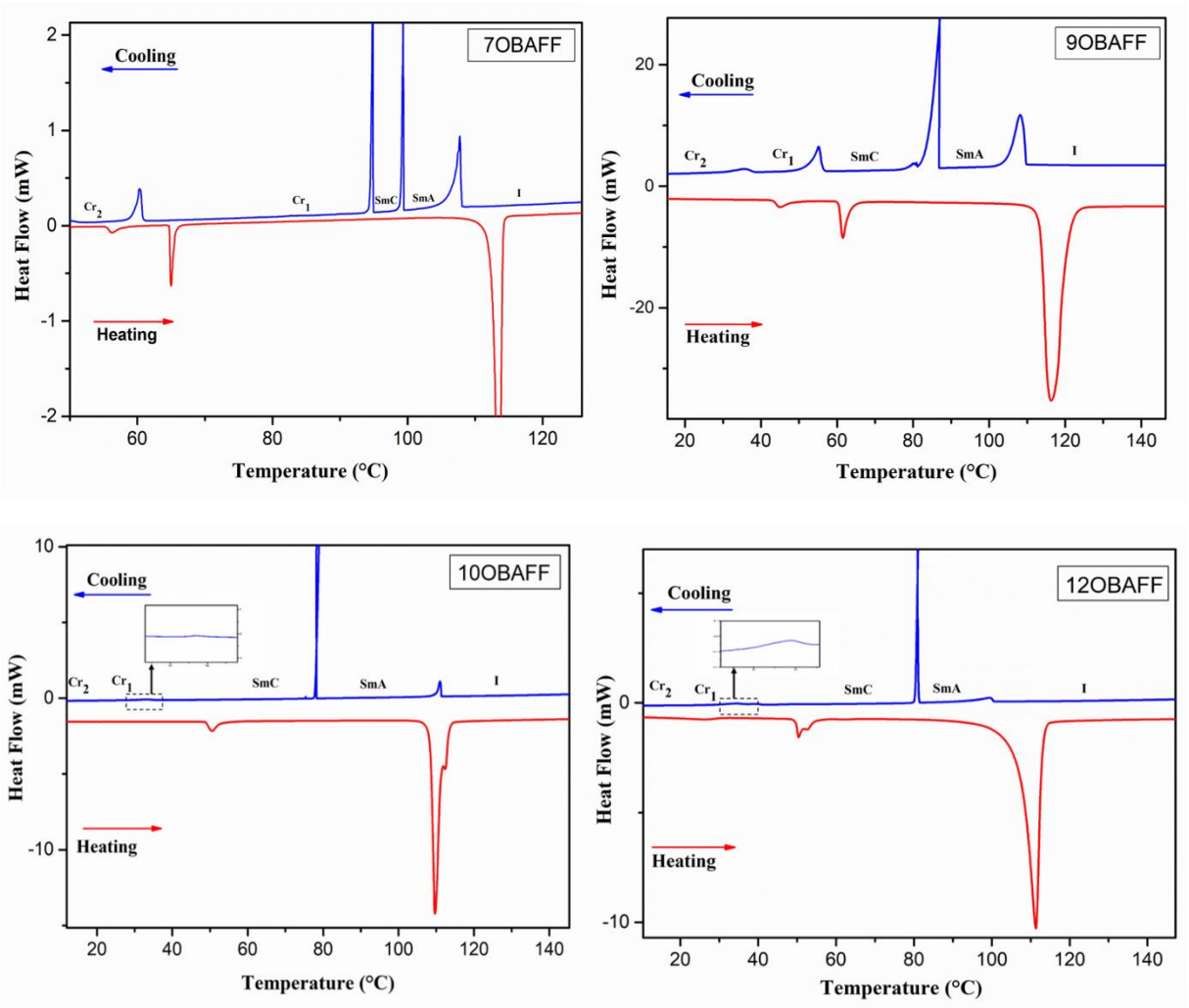

Figure S1. The second DSC cycles of nOBAFF upon heating and cooling.

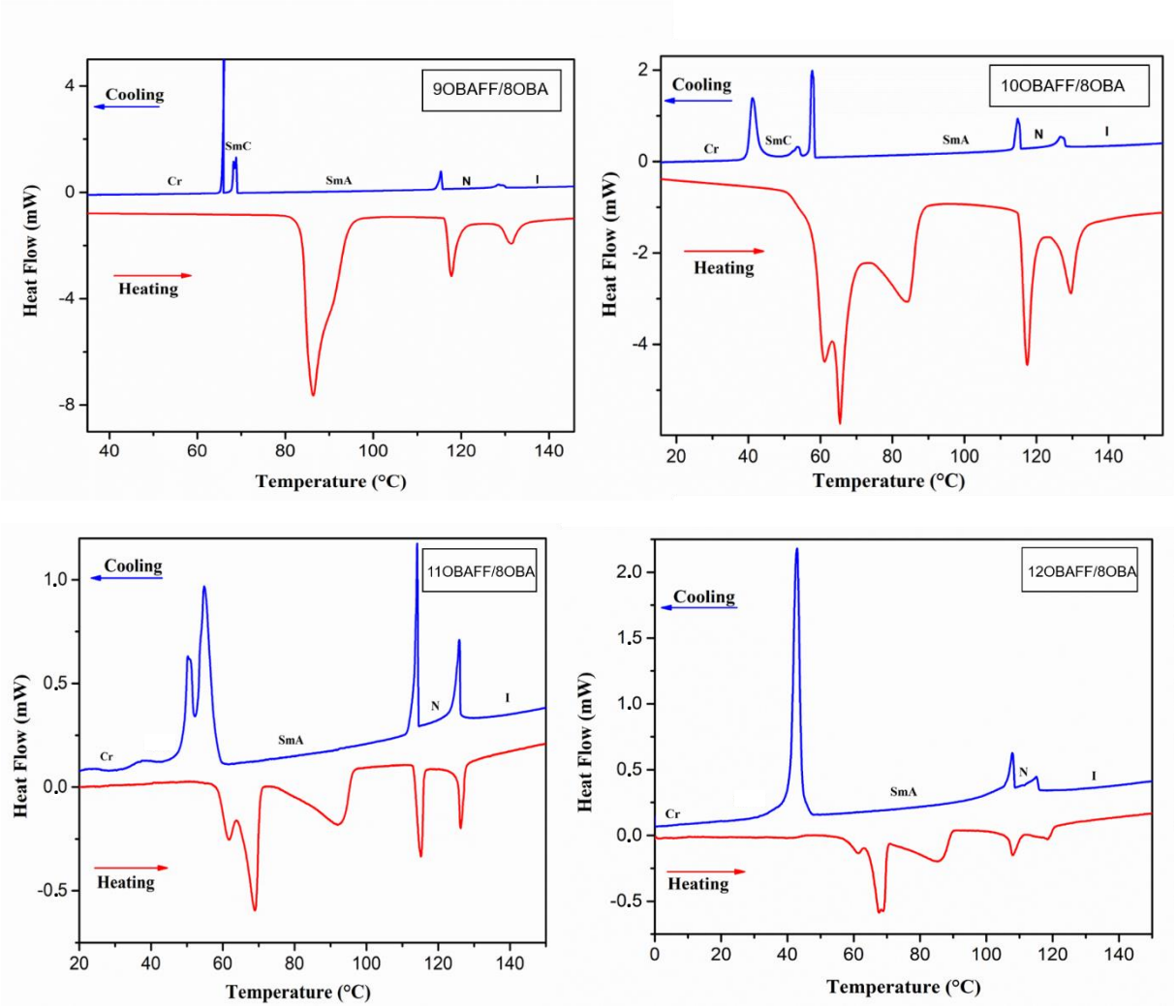

Figure S2. The second DSC cycles of nOBAFF/8OBA upon heating and cooling.